Hindawi
Mathematical Problems in Engineering
Volume 2019, Article ID 2301714, 17 pages
https://doi.org/10.1155/2019/2301714

Research Article

Synergistic Design of the Bipedal Lower-Limb through Multiobjective Differential Evolution Algorithm

Jesús S. Pantoja-García,[1] Miguel G. Villarreal-Cervantes,[1] Consuelo V. García-Mendoza,[2] and Víctor M. Silva-García[1]

[1]*Postgraduate Department, Mechatronic Section, Optimal Mechatronic Design Laboratory, CIDETEC, Instituto Politécnico Nacional, Mexico City 07700, Mexico*
[2]*ESCOM, Instituto Politécnico Nacional, Mexico City 07700, Mexico*

Correspondence should be addressed to Miguel G. Villarreal-Cervantes; villamike@hotmail.com

Received 7 January 2019; Revised 4 April 2019; Accepted 15 April 2019; Published 2 May 2019

Academic Editor: Erik Cuevas

The complexity in the design of bipedal robots has motivated the use of simple mechanisms to accomplish the desired locomotion task with a minimum control effort. Nevertheless, a diverse set of conflictive design criteria must be met to develop the bipedal gait. In this paper, the synergy in the eight-bar mechanism design criteria to satisfy the bipedal lower-limb behavior is promoted by proposing a Pareto-based Nonlinear Mixed Discrete-Continuous Constrained Multiobjective Optimization Problem and by improving the search in the optimizer through the inclusion of the Multiselection Strategy into the multiobjective differential evolution algorithm, where the conflictive design objectives are the continuous path generation based on an approximation error to track twenty precision points of the bipedal gait and also the force transmission exerted when the foot reaches the ground. The manufacture of a prototype with a specific design trade-off experimentally validates the obtained synergistic design with the proposed design approach. In addition, the empirical analysis in simulation through a statistical validation indicates that the Multiselection Strategy explores and exploits the design solutions promoting the diversity, convergence, and capacity features of the obtained Pareto front with respect to other four multiobjective optimizers and consequently improves the reconfigurability in the design such that more alternatives result to the designer decision making.

1. Introduction

Human beings have handled and solved significant problems throughout history, producing theories and technologies even more sophisticated [1]. One of these theoretical and practical aspects is focused on the development of high-performance bipedal robots in terms of energy consumption, design complexity, number of actuators, and so on. Despite the complexity in their mechanical design (interrelation of several aspects: temporal-spatial data, kinematic variables, and the like), a significant challenge in the design of bipedal robots is to develop it as simple as possible implying a prototype with low cost, low energy consumption, and easy to control.

In that way, there has been a growing interest in the design of bipedal robots focus mainly on lower-limb rehabilitation [2] and lower-limb prostheses [3, 4]. Furthermore, several design studies that involve simple mechanisms have been exploited to reproduce the human gait: six-bar mechanism [5], Chebyshev mechanism [6], and ten-bar mechanism [7]. Nevertheless, the limitation of the linkage mechanism to generate continuous paths is that the desired continuous path can only be generated approximately and then, in some of cases, optimization approaches have been stated to satisfy several precision points of designs. The optimization problem was solved by using meta-heuristic algorithms instead of gradient-based approaches because the latter are problem dependent (the convergence to a solution is only guaranteed for continuous problem); they present high sensitivity to initial condition which results in the convergence to diverse local minima in multimodal optimization problems, and they require the gradient of the performance function and/or constraints which is not always possible for real-world applications. For instance, Calva et al. [8] synthesized

a reconfigurable four-bar linkage to the rehabilitation gait in children with cerebral palsy. A mono-objective constrained optimization problem was formulated and solved by differential evolution (DE) and Sequential Quadratic Programming (SQP) techniques. The DE meta-heuristic algorithm provided a better performance than the SQP gradient-based approach due to the fact that the former efficiently explores the search space in the constrained problem.

Therefore, meta-heuristic approaches are gaining more attention lately [9, 10] because they can find solutions near to the optimum, be less prone to get stuck in local minima due to the fact that they are population-based approaches, are merged to other techniques to improve the performance, and are used in nonlinear, discontinuous, continuous-discrete problems. Approaches that employed meta-heuristic algorithms have been recently developed in the design of rehabilitation robots based on mechanisms. Shao et al. [11] performed the dimensional synthesis of a cam-linkage mechanism to human gait rehabilitation, considering a multiobjective optimization problem. A weighed sum approach was used to transform the multiobjective optimization problem into a mono-objective one. This problem was solved via genetic algorithm. The main proposal advantage is that the two-degree-of-freedom in the initial design was effectively reduced to a one-degree-of-freedom cam-linkage mechanism. The results proved that the final design was capable of tracking the desired path. Bataller et al. [12] synthesized an exoskeleton for hand finger rehabilitation through a low-cost mechanism. The objective designs were the deviation of the generated path, as well as the difference of the three angles of each phalanx. The authors handled the optimization problem with the weighted sum approach which was solved by Malaga University Mechanism Synthesis Algorithm. In order to validate the design, a 3D-printed prototype was manufactured. Ji and Manna [13] synthesized a planar four-bar mechanism to track a closed ankle trajectory obtained from gait data. By establishing and solving a mono-optimization problem was possible to find a design which minimizes the trajectory tracking error. A conceptual design of the linkage mechanism was displayed to expose the idea of creating machines using planar mechanisms. McDaid [14] performed a two degree-of-freedom five-bar linkage to reinstate walking patterns for children with cerebral palsy, to which, a multiobjective optimization problem was formulated and solved via genetic algorithm with a weighted sum approach. The design was experimentally validated with four healthy subjects, as well as with clinical data from three children with cerebral palsy. Singh et al. [15] proposed a novel synthesis method, considering a two-stage mono-objective optimization problem and applying to a four-bar exoskeleton lower-limb to mimic the human gait. The first stage involves the tracking error between the generated and desired trajectories for the design a four-bar linkage. In the second stage the configurations of the linkage for the remaining precision points are determined. A conceptual design of an exoskeleton demonstrated the viability of the method. In [16], the same authors synthesized a crank-rocker planar mechanism (human knee-exoskeleton) by formulating a constrained mono-objective optimization problem with the error between generated and prescribed trajectory as the performance function. The optimization problem was solved by teaching-learning-based-optimization algorithm, considering the penalty method to manage all the constraints. A prototype was used to validate the design, observing that a subject was able to walk smoothly with the knee-exoskeleton designed. Shen et al. [17] proposed an integrated method of type and dimensional synthesis to design one degree-of-freedom mechanisms with only revolute joints based on the four-bar mechanisms. During the design process a mono-objective optimization problem is formulated and solved via genetic algorithms. The proposed method was applied to a leg exoskeleton for hip and knee joint gait reproduction and a finger exoskeleton for curling motion duplication. Pantoja et al. [18] synthesized an eight-bar-one-degree-of-freedom mechanism to track a trajectory similar to the human gait on sagittal plane. A mono-objective optimization problem was formally stated to fulfill the design requirement. Experimental results verified the design approach through a 3D-printed prototype.

An important aspect to be considered in the bipedal design is how to synergistically improve the trade-offs in the design criteria. In previous works related to simple bipedal design the trade-off among design criteria is a priori given through weighted sum approach. Nevertheless, once the weights are set in the weighted sum approach, a specific trade-off is found such that the reconfigurability of the design can not be achieved [19]. In addition, it is quite impossible to obtain the suitable synergy between different design criteria because an evenly distributed set of weights do not produce a uniform distribution of the Pareto front points [20]. Then, to perform an efficient synergy among design criteria in the bipedal lower-limb design, a Pareto-based Multiobjective Optimization Problem [10] must be considered to efficiently search several trade-offs for the specific application. Moreover, the optimization technique to be used in the synergistic design is also a crucial factor to find the appropriate trade-offs in the design with several criteria [21]. Due to the features and properties of the problem, there is not a universal algorithm that performs better for all classes of multiobjective optimization problems [22]. Hence, to find the best synergy in the design implies the inclusion of strategies which promotes an efficient exploration and exploitation of the design space to fulfill diverse trade-offs in the design.

Therefore, in this paper, the synergistic design of a bipedal lower-limb through a one-degree-of-freedom eight-bar mechanism is accomplished by (i) *Proposing a Pareto-based Nonlinear Mixed Discrete-Continuous Constrained Multiobjective Optimization Problem (NMDC-CMOOP)*. The proposed synergistic design approach integrates the continuous path generation based on the tracking of twenty precision points of the bipedal gait and the force transmission (via transmission angle) exerted in the stance phase. (ii) *Including a Multiselection Strategy into the selection stage of the multiobjective differential evolution algorithm*. This strategy explores specific regions of the search space and promotes to discover a large amount and spread of Pareto solutions, providing more and better alternatives to the designer decision

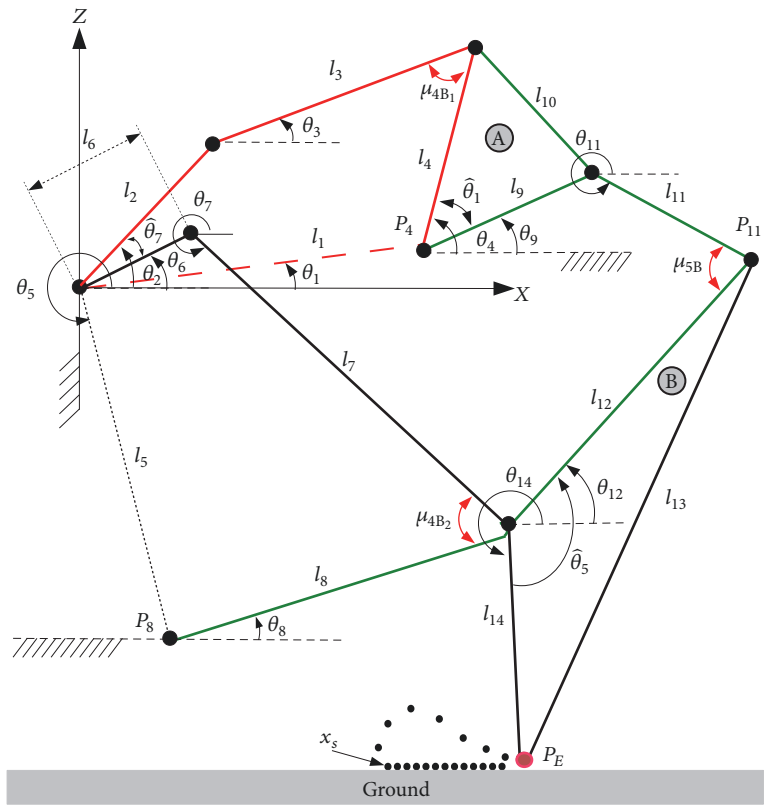

Figure 1: Bipedal lower-limb mechanism.

making (more reconfigurability in the bipedal lower-limb design).

The paper is organized in the following way: Section 2 presents the kinematic model of the Bipedal Lower-Limb (BLL). The objective functions, the design variables, and the constraints involved in the Nonlinear Mixed Discrete-Continuous Constrained Multiobjective Optimization Problem are explained in Section 3. Section 4 explains the proposed algorithm to solve the NMDC-CMOOP. Section 5 covers an assessment of the effectiveness of the proposed DE-based selection strategy algorithm and other four algorithms. Besides, experiments of the best mechanism found are conducted to verify the synergistic design. Finally, in Section 6 the conclusions are drawn.

2. Analysis of the Bipedal Lower-Limb

Two identical mechanisms are required to generate the human gait on the sagittal plane, where each is a bipedal lower-limb. However, it is sufficient to design only one element instead of the two required due to the symmetrical behavior of the gait. Therefore, the one degree-of-freedom eight-bar planar mechanism presented in Figure 1 is designed to generate the human gait path on the sagittal plane. The link lengths is grouped in the vector $\vec{l} = (l_1, l_2, \ldots, l_{14})$, the link angular displacements are represented as $\vec{\theta} = (\theta_1, \theta_2, \ldots, \theta_{14})$, the terms $\widehat{\theta}_1, \widehat{\theta}_5$ are the interior angles of the triangular links marked as A and B, and the Cartesian coordinate $P_E = [x_E, z_E]$ corresponds to the point where the desired gait movement would be set. This mechanism is selected due to its scalable design, energy efficiency, bioinspired locomotion, and it has a wide operation range capable of generating closed-loop trajectories [23].

2.1. Kinematic Model. Separating the BLL into three sub-mechanisms (i.e., two four-bar and one five-bar mechanism), kinematics equations are derived in (1) and (2) from [18].

$$\theta_{j+k} = 2\text{atan2}\left(\frac{-\widehat{B} + m_{4b_\alpha}(-1)^{\beta}\sqrt{\widehat{B}^2 + \widehat{A}^2 - \widehat{C}^2}}{\widehat{C} - \widehat{A}}\right) \quad \forall j = 0, 4 \wedge k = 3, 4 \tag{1}$$

$$\theta_{o+11} = 2\text{atan2}\left(\frac{-\overline{B} + m_{5b}(-1)^{o}\sqrt{\overline{B}^2 + \overline{A}^2 - \overline{C}^2}}{\overline{C} - \overline{A}}\right) \quad \forall o = 0, 1 \tag{2}$$

where

$$\alpha = \frac{(j-2)^j}{\left(\sqrt[4]{j+4}\right)^j}$$

$$\beta = (j + k + 1)$$

$$\widehat{A} = (-1)^k 2 l_{j+1} l_{j+k} \cos\left(\theta_{j+1}\right)$$

$$
\begin{aligned}
&+(-1)^{k+1}\,2l_{j+2}l_{j+k}\cos\left(\theta_2\right)\\
\widehat{B} &= (-1)^{k}\,2l_{j+1}l_{j+k}\sin\left(\theta_{j+1}\right)\\
&+(-1)^{k+1}\,2l_{j+2}l_{j+k}\sin\left(\theta_2\right)\\
\widehat{C} &= l_{j+1}^2+l_{j+2}^2+(-1)^{k+1}\,l_{j+3}^2+(-1)^{k}\,l_{j+4}^2\\
&-2l_{j+1}l_{j+2}\cos\left(\theta_{j+1}-\theta_2\right)\\
\overline{A} &= (-1)^{o+1}\,2l_{o+11}l_{8(1-o)+15o}\cos\theta_{8(1-o)+15o}\\
&+(-1)^{o}\,2l_9l_{o+11}\cos\theta_9\\
&+(-1)^{o+1}\,2l_{o+11}l_{8o+15(1-o)}\cos\theta_{8o+15(1-o)}\\
\overline{B} &= (-1)^{o+1}\,2l_{o+11}l_{8(1-o)+15o}\sin\theta_{8(1-o)+15o}\\
&+(-1)^{o}\,2l_9l_{o+11}\sin\theta_9\\
&+(-1)^{o+1}\,2l_{o+11}l_{8o+15(1-o)}\sin\theta_{8o+15(1-o)}\\
\overline{C} &= l_8^2+l_9^2+l_{o+11}^2+l_{15}^2-l_{12-o}^2\\
&+(-1)^{o+1}\,2l_8l_{9(1-o)+15o}\cos\left(\theta_8-\theta_{9(1-o)+15o}\right)\\
&+(-1)^{o}\,2l_8l_{9o+15(1-o)}\cos\left(\theta_8-\theta_{9o+15(1-o)}\right)\\
&-2l_9l_{15}\cos\left(\theta_9-\theta_{15}\right)
\end{aligned}
\tag{3}
$$

3. Synergistic Design of the BLL

The design of the BLL takes into account the synergy between the generation of the human gait path on the sagittal plane and the force transmission from the input link to the output point PE. Therefore, in order to fulfill a synergistic design approach with different trade-offs, a multiobjective optimization problem is stated as a mathematical programming problem, where (4) and (5) show its general representation.

$$\min \quad \left[f_1\left(\vec{x}\right), f_2\left(\vec{x}\right)\right] \tag{4}$$

subject to

$$
\begin{aligned}
g_i\left(\vec{x}\right) &\le 0 \quad i=1,2,\ldots,m\\
h_i\left(\vec{x}\right) &= 0 \quad i=1,2,\ldots,p
\end{aligned}
\tag{5}
$$

where

$\vec{x}$: vector of design variables;

m: number of inequality constraints;

p: number of equality constraints.

In the next sections, the functions related in the multiobjective optimization problem for the synergistic design of the BLL are detailed.

3.1. Design Objectives. The first design objective f_1 displayed in (6) is related to the accuracy of the path tracking. This considers the error between the desired path $\overline{P}_E = [x_E, \overline{z}_E]$ and the Cartesian coordinates tracked by the point $P_E = [x_E, z_E]$, where $\overline{n}$ is the number of precision points to satisfy the point $\overline{P}_E$ of the BLL. The second criterion f_2 displayed in (7) provides a design with the most suitable force transmission during the stance phase of the BLL and also is less prone to inaccuracies due to manufacturing errors, thermal expansion, or material contraction. Then, the second design objective is the deviation of the transmission angle of the three submechanisms $\mu_\varrho \mid \varrho = \{4B_1, 4B_2, 5B\}$ from the ideal one (pressure angle [25]).

$$f_1 = \sum_{i=1}^{\overline{n}}\left(\overline{x}_E^i - x_E^i\right)^2 + \sum_{i=1}^{\overline{n}}\left(\overline{z}_E^i - z_E^i\right)^2 \tag{6}$$

$$f_2 = \left(\mu_{4B_1}-\frac{\pi}{2}\right)^2 + \left(\mu_{4B_2}-\frac{\pi}{2}\right)^2 + \sum_{j=12}^{\overline{n}}\left(\mu_{5B}-\frac{\pi}{2}\right)^2 \tag{7}$$

where

$$
\begin{aligned}
x_E^i &= l_6\cos\theta_2^i + l_7\cos\theta_7^i + l_{14}\cos\theta_{14}^i\\
z_E^i &= l_6\sin\theta_2^i + l_7\sin\theta_7^i + l_{14}\sin\theta_{14}^i\\
\mu_{4B_1} &= \cos^{-1}\left(\frac{l_3^2+l_4^2-\left(l_1-l_2\right)^2}{2l_3l_4}\right)\\
\mu_{4B_2} &= \cos^{-1}\left(\frac{l_7^2+l_8^2-\left(l_5-l_6\right)^2}{2l_7l_8}\right)\\
\mu_{5B} &= \theta_{12}^j - \theta_{11}^j + 2\pi
\end{aligned}
\tag{8}
$$

3.2. Design Variables. The design variables of the BLL are the link lengths $l_i\ \forall i = 1,2,\ldots,9,11,12,14$, the angles θ_1, θ_5 of the fixed links, the interior angles $\widehat{\theta}_1, \widehat{\theta}_5$ of the triangular links, the angle deviation $\widehat{\theta}_7$, the start coordinate x_s of the gait path, kinematic configurations of submechanisms $m_b = \{m_{4b_1}, m_{4b_2}, m_{5b}\}$ (elbow up and elbow down configuration), and the $\overline{n}$ angular displacements of the crank $\theta_2 = \{\theta_2^i \mid i = 1,2,\ldots,\overline{n}\}$. Finally, the vector $\vec{x}$ in (9) collects the design variables, where the discrete variables are given by m_b and the rest consists of real (continuous) ones.

$$\vec{x} = \left(l_i, \theta_1, \theta_5, \widehat{\theta}_1, \widehat{\theta}_5, \widehat{\theta}_7, x_s, m_b, \theta_2\right)^T \in R^{21+\overline{n}} \tag{9}$$

3.3. Constraints

3.3.1. Lower and Upper Bounds of Design Variables. Bounds on design variables delimit the search space to finding an optimal solution in real-world engineering problems. Such bounds are set as inequality constraint in (10), where the upper and lower limits are given in Table 1. It is important to note that the variables m_b can only take the discrete values of −1 or 1.

$$\vec{x}_l \le \vec{x} \le \vec{x}_u \tag{10}$$

Table 1: Bounds of the design variables.

Bounds	l_i	θ_1	θ_5	$\widehat{\theta}_1$	$\widehat{\theta}_5$	$\widehat{\theta}_7$	$\overline{x}_s$	m_b	θ_2
$\overrightarrow{x}_l$	0	0	0	0	0	0	$-1/2$	-1	0
$\overrightarrow{x}_u$	0.2	2π	2π	π	π	2π	$1/2$	1	2π

Table 2: Hip angles ($\widetilde{\theta_1}$) and knee angles ($\widetilde{\theta_2}$) obtained from [24].

$\overline{n}$	$\widetilde{\theta_1}$	$\widetilde{\theta_2}$	$\breve{\theta}_1$	$\breve{\theta}_2$	$\overline{n}$	$\widetilde{\theta_1}$	$\widetilde{\theta_2}$	$\breve{\theta}_1$	$\breve{\theta}_2$
1	27.9	8.8	27.9	8.8	11	−7	9.7	−7	9.7
2	27.6	12.9	27.6	12.9	12	−10.2	11.1	−10.2	11.1
3	26.6	19	26.6	19	13	−12.5	14.4	−12.5	14.4
4	23.9	22.1	23.9	22.1	14	−11.8	29	27.3	16.1
5	19.8	21.6	19.8	21.6	15	−1.9	50.8	23	22.2
6	15.1	19.3	15.1	19.3	16	12.2	65.3	15.1	19.3
7	10.3	16.5	10.3	16.5	17	23.4	61.9	6.7	14.6
8	5.5	13.9	5.5	13.9	18	29.4	44.4	−1.3	10.7
9	0.9	11.6	0.9	11.6	19	29.5	19.2	−7.9	9.9
10	−3.3	10	−3.3	10	20	27.5	5.5	−12.5	14.4

3.3.2. Grashof Criterion. Another constraint in the design of the BLL is the Grashof criterion of the four-bar submechanisms [26], which states *if the sum of the shortest and longest link lengths is less than or equal to the amount of the two remaining links, then at least one of them can rotate completely*. This criterion is set as inequality constraints in (11) and (12).

$$g_1 : l_2 + l_1 - l_3 - l_4 < 0 \tag{11}$$

$$g_2 : l_6 + l_5 - l_7 - l_8 < 0 \tag{12}$$

Besides, the four-bar submechanisms can be locked if the inequality constraints (13)-(16) are not taken into account. These constraints force that such mechanisms present crank-rocker configuration.

$$g_3 : -l_4 - l_1 + l_2 + l_3 < 0 \tag{13}$$

$$g_4 : -l_3 - l_1 + l_2 + l_4 < 0 \tag{14}$$

$$g_5 : -l_8 - l_5 + l_6 + l_7 < 0 \tag{15}$$

$$g_6 : -l_7 - l_5 + l_6 + l_8 < 0 \tag{16}$$

3.3.3. Functional Morphology. The functional morphology constraint is associated with the conditions that the BLL can move freely (i.e., without any of its joints hitting the ground). The inequality constraints given in (17)-(19) force that the points $P_4 = [P_{4x}, P_{4z}]$, $P_8 = [P_{8x}, P_{8z}]$, and $P_{11} = [P_{11x}, P_{11z}]$ are above of the point P_E where the path is performed.

$$g_7 : -P_{11z} - 0.25 < 0 \tag{17}$$

$$g_8 : -P_{8z} - 0.25 < 0 \tag{18}$$

$$g_9 : -P_{4z} - 0.25 < 0 \tag{19}$$

where

$$\begin{aligned} P_{4z} &= l_1 \sin(\theta_1) \\ P_{8z} &= l_5 \sin(\theta_5) \\ P_{11z} &= l_6 \sin(\theta_6) + l_7 \sin(\theta_7) + l_{12} \sin\theta_{12} \end{aligned} \tag{20}$$

3.3.4. Real Kinematic Movement. This set of constraints does not allow that submechanisms present nonphysical design (i.e., mechanisms that do not satisfy the closed kinematic chain). Then, each of the $\overline{n}$ crank input angular motions θ_2 must guarantee that constraints (21) and (22) are satisfied to produce the motion in the point P_E of the BLL.

$$g_{9+i} : \widehat{B}^2 + \widehat{A}^2 - \widehat{C}^2 \geq 0 \quad \forall i = 1, \ldots, \overline{n} \tag{21}$$

$$g_{9+\overline{n}+j} : \overline{B}^2 + \overline{A}^2 - \overline{C}^2 \geq 0 \quad \forall j = 1, \ldots, \overline{n} \tag{22}$$

3.3.5. Desired Path. The desired path $\overline{P}_E = [\overline{x}_E, \overline{z}_E]$ uses the sign convention in Figure 2 for the hip $\widetilde{\theta}_1$ and knee $\widetilde{\theta}_2$ angles of the lower-limb of human being. Moreover, this path includes the torso movement $H(x_h, z_h)$ (see Figure 3). Then, the desired path is parameterized and resized in (23) considering the hip-knee angles presented in the biomechanical study in [24]. Twenty hip-knee angles of a younger group between 6 to 12 years old collected from such study are used and shown in Table 2. As a result, the precision point number for the desired path is $\overline{n} = \overline{n}_a + \overline{n}_b = 20$, where $\overline{n}_a = 13$ means that 65% of the gait cycle is in the stance phase, and $\overline{n}_b = 7$ means that 35% of the gait cycle is in the swing phase.

The desired path expressed in (23) is included as inequality constraints, taken into account the lengths $\widetilde{l}_1 = 0.416m$ and $\widetilde{l}_2 = 0.418m$ and the scale factors $f_x = 0.0001125$ and $f_z = 0.00025$ yielding a gait path with a step length of about $0.08m$ and a step elevation of about $0.04m$. It is important to note that this path presents a closed form, and an importance

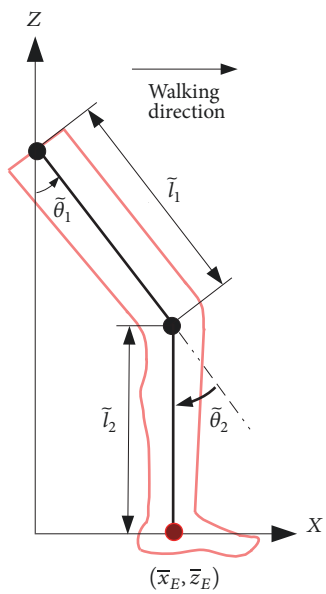

FIGURE 2: Walking model and sign convention.

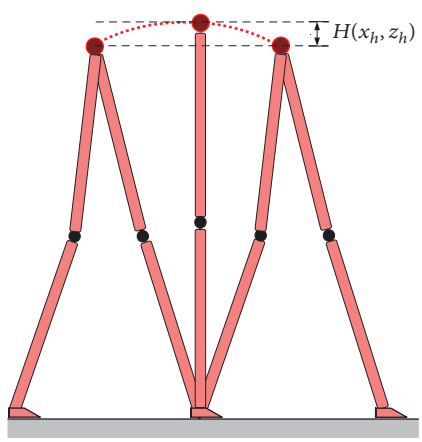

FIGURE 3: Vertical displacement of the torso H.

challenge in the bipedal lower-limb design is to track this two degree-of-freedom $d.o.f$ Cartesian space trajectory with one $d.o.f$ eight-bar mechanism.

$$\overline{P}_E^{\pi} \begin{cases} \bar{x}_E = \left(x_h + \tilde{l}_1 \sin\left(\tilde{\theta}_1\right) + \tilde{l}_2 \sin\left(\tilde{\theta}_1 - \tilde{\theta}_2\right) + 400\right) f_x \\ \bar{z}_E = \left(z_h - \tilde{l}_1 \cos\left(\tilde{\theta}_1\right) - \tilde{l}_2 \cos\left(\tilde{\theta}_1 - \tilde{\theta}_2\right)\right) f_z - 0.3 \end{cases} \tag{23}$$

where

$$\begin{aligned} x_h &= 0 \\ z_h &= \tilde{l}_1 \cos\left(\breve{\theta}_1\right) + \tilde{l}_2 \cos\left(\breve{\theta}_1 - \breve{\theta}_2\right) \end{aligned} \tag{24}$$

4. Multiobjective Differential Evolution Algorithm

Differential Evolution (DE) proposed by Price and Storn in 1995 [27] is a population-based meta-heuristic global search technique. DE is formulated to solve numerical optimization problems coded with real values as in evolution strategies. In the same way as evolutionary algorithms, DE presents operators of recombination, mutation, and selection strategies. DE has had a remarkable acceptance in the diverse areas such as mechanical engineering design [28], mechatronic design [21], automatic control tuning [29], and so on. This fact is because of the suitable convergence and robustness properties, the reduced number of tuning parameters, and the success in solving real-world applications. Nevertheless, the search capability of DE may be compromised in multimodal problems [30]. Accordingly, further improvements must be made to enhance (avoid stagnation to local optima) its performance for a particular optimization problem.

The DE process consists of three stages: mutation, crossover, and selection. In the mutation process, the individuals NP in the population change the search direction based on the distribution of three solutions and the step size F, as is shown in

$$v_{i,j} = x_{r3} + F\left(x_{r1} - x_{r2}\right) \tag{25}$$

In the recombination process (26), some design parameters of parent individuals $\vec{x}_{i,G}$ and mutant vectors $\vec{v}_{i,G}$ share their genetic information to generate the offspring population $\vec{u}_{i,G}$. The parameter C_r influences the probability to obtain information from either parent or the offspring (great values mean less impact of the parent individual).

$$u_{i,j,G} = \begin{cases} v_{i,j,G} & if \ \left(\text{rand}_j(0,1) \le C_r \text{ or } j = j_{rand}\right) \\ x_{i,j,G} & \text{otherwise} \end{cases} \tag{26}$$

The generated offspring competes against of its corresponding parent and the most competitive survives to the next generation. The mechanism to know the most suitable individual is based on the proposed Multiselection Strategy explained in the next section. This strategy promotes a better convergence as well as widespread solutions in the Pareto front. Additionally, based on [31], the crowding distance strategy [32] and an External Archive (ExA) are employed to keep the best individuals (based on Pareto dominance) through the optimization process, allowing promoting diversity in the solutions. This strategy interchanges individuals stored in the ExA to provide the information to the mutation process, meaning that the individuals required in the mutation process are taken from the current population or from the ExA, depending on the Normal Selection (NS) value. This process is repeated until a maximum number of generations G_{max} is fulfilled.

Algorithm 1 displays the DE-based approach with the Multiselection Strategy.

The discrete variables in $\vec{m_b}$ of the design variable vector $\vec{x}$ (9) are handled as in (27); i.e., once the discrete design variable is generated (randomly generated in the population initialization in line 1 or after the crossover process in line 14 of the Algorithm 1) the procedure in (27) is performed.

$$\vec{m_b} = \begin{cases} +1 & if \ \left(x_{i,j} > 0\right) \\ -1 & \text{otherwise} \end{cases} \tag{27}$$

1: Create a random initial population $\vec{x}_l \leq \vec{X}_0 \leq \vec{x}_u$, and $ExA = \emptyset$
2: Evaluate X_0 in performance functions.
3: $G \longleftarrow 0$
4: **while** $G \leq G_{max}$ **do**
5: **for** i to NP **do**
6: **if** $G <= NS \times G_{max}$ **then**
7: Select randomly $r_0 \neq r_1 \neq r_2 \neq i$
8: **else**
9: Choose $\vec{x}_{r1}$, $\vec{x}_{r2}$ and $\vec{x}_{r3}$ from ExA
10: **end if**
11: $j_{rand} = randint[1, D]$
12: **for** j to D **do**
13: **if** $rand_j < [0, 1]$ or $j = j_{rand}$ **then**
14: $u_{i,j} = x_{r3,j} + F(x_{r1,j} - x_{r2,j})$
15: **else**
16: $u_{i,j} = x_{i,j}$
17: **end if**
18: **end for**
19: Multi-Selection Strategy between $\vec{x}_i$ and $\vec{u}_i$ based on Algorithm 2
20: Update the ExA with the information of the best performance individuals.
21: $G \longleftarrow G + 1$
22: **end for**
23: **end while**

Algorithm 1: Multiselection Strategy DE-based.

4.1. Proposed Multiselection Strategy. Some concepts related to multiobjective problems are firstly given to describe the proposed Multiselection Strategy (MSS).

Definition 1. Let $\vec{x} \in \Omega$ be the full set of alternatives for the decision variables, the feasible region is such that $\mathbb{F} = \{\vec{x} \in \Omega \mid g(\vec{x}) < 0,\ h(\vec{x}) = 0\}$.

Definition 2. Given two vectors $\vec{x}, \vec{x'} \in \mathbb{R}^{n_J}$, we say that $\vec{x}$ dominates $\vec{x'}$ (denoted by $\vec{x} \prec \vec{x'}$) if $\vec{x}_i \leq \vec{x}_i'$ & $\vec{x} \neq \vec{x'}$, for $i = 1, 2, \ldots, n_J$.

Definition 3. A vector of decision variables $\vec{x^*} \in \mathbb{F}$ is Pareto-optimal if it is nondominated with respect to $\mathbb{F}$.

Definition 4. The Pareto-optimal set P^* is defined by

$$P^* = \left\{\vec{x} \in \mathbb{F} \mid \vec{x} \text{ is Pareto-optimal}\right\} \tag{28}$$

Definition 5. The Pareto Front PF^* is defined by

$$PF^* = \left\{f\left(\vec{x}\right) \in \mathbb{R}^2 \mid \vec{x} \in P^*\right\} \tag{29}$$

The proposed MSS promotes the spread, diversity, convergence, and capacity [33] of the solutions through the Pareto front to provide a diverse set of bipedal lower-limb designs that fulfill different trade-offs between design objectives. This strategy splits the population of NP individuals into two subpopulations with the same number of individuals named as Virtual Subpopulation 1 (VS1) and Virtual Subpopulation 2 (VS2). Each subpopulation implements different selection processes. The VS1 enhances the convergence and the spread of a relevant region of the Pareto front (exploitation), and the VS2 explores the solutions space to promote diversity (exploration) in the search. This strategy is included when the offspring and the parent competes (line 19 of Algorithm 1). The MSS follows the following rules:

(1) Any feasible solution is preferable over any unfeasible solution.

(2) If the two solutions are feasible,

the nondominated one is preferred;
if both solutions are nondominated, then

Individuals in VS1:

(i) The one having the smallest value of f_1 is preferred.

Individuals in VS2:

(ii) One of them is chosen considering the same probability to be selected (flip a coin).

(3) Among two unfeasible solutions, the one having a smaller constraint violation is preferred.

Algorithm 2 displays the proposed selection. The MSS is similar to the Deb Criterion [34]; however the main differences are the way in which both individuals are nondominated. The VS1 searches in the improvement of the performance function f_1 (path tracking accuracy) as can be seen in line 9 of the Algorithm 2, while VS2 promotes

1: Virtual split of X into: $X_i^1 \quad \forall i = 1, 2, 3, ..., NP/2$, $X_i^2 \ \forall i = NP/2 + 1, ..., NP$
2: **if** $\overrightarrow{u_i} \in \mathbb{F} \& \overrightarrow{x_i} \notin \mathbb{F}$ **then**
3: $\quad \overrightarrow{x_{i,G+1}} = \overrightarrow{u_{i,G}}$
4: **else if** $\overrightarrow{u_i} \in \mathbb{F} \& \overrightarrow{x_i} \in \mathbb{F}$ **then**
5: $\quad$ **if** $f(\overrightarrow{u_i}) \prec f(\overrightarrow{x_i})$ **then**
6: $\quad\quad \overrightarrow{x_{i,G+1}} = \overrightarrow{u_{i,G}}$
7: $\quad$ **else**
8: $\quad\quad$ Whether $X \in X^1$: ▷VS1
9: $\quad\quad$ **if** $f_1(\overrightarrow{u_i}) \leq f_1(\overrightarrow{x_i})$ **then**
10: $\quad\quad\quad \overrightarrow{x_{i,G+1}} = \overrightarrow{u_{i,G}}$
11: $\quad\quad$ **end if**
12: $\quad\quad$ Whether $X \in X^2$: ▷VS2
13: $\quad\quad$ Random choice between $\overrightarrow{x_{i,G+1}}$ and $\overrightarrow{u_{i,G}}$
14: $\quad$ **end if**
15: **else if** $\overrightarrow{u_i} \notin \mathbb{F} \& \overrightarrow{x_i} \notin \mathbb{F}$ **then**
16: $\quad$ Choose the one with the smaller constraint violation i.e., $\sum_{i=1}^{NP} \max(0, \text{sign}(g(\overrightarrow{u_i})))$ vs $\sum_{i=1}^{NP} \max(0, \text{sign}(g(\overrightarrow{x_i})))$.
17: **else**
18: $\quad \overrightarrow{x_{i,G+1}} = \overrightarrow{x_{i,G}}$
19: **end if**

Algorithm 2: Proposed Multiselection Strategy.

1: **Begin**
2: $\quad CD(j) = 0 \ \forall j = \{1, \ldots, S_F\}$
3: $\quad$ Sort in descent order the non-dominated set.
4: $\quad CD_m(1) = \infty$ and $CD_m(S_F) = \infty$.
5: $\quad$ **for** $i = 1$ to m **do**
6: $\quad\quad$ **for** $j = 2$ to $S_F - 1$ **do**
7: $\quad\quad\quad CD_m(j) = CD_m(j) + \left\| \dfrac{\overrightarrow{z}_i(j+1) - \overrightarrow{z}_i(j-1)}{\overrightarrow{z}_i^{max} - \overrightarrow{z}_i^{min}} \right\|$
8: $\quad\quad$ **end for**
9: $\quad$ **end for**
10: **End**

Algorithm 3: Crowding distance.

a random search into the design space; i.e., any solution is chosen with the equal probability to be selected (observe line 13 of the Algorithm 2).

The MSS encourages a Pareto front more widespread towards the interest regions (to minimize f_1) of designer interest and also promotes more synergistic solutions because different trade-offs are found in the region of interest.

4.1.1. Promoting Diversity. The diversity of the Pareto front is promoted in the DE algorithm by using the diversity strategy introduced by the Crowding Distance (CD) in [31]. The CD estimates the perimeter of the nearest neighbors of each solution. Algorithm 3 shows how to compute the crowding distance. The Normal Selection (NS) parameter is introduced to change the selection of vectors in the mutation process. When the generation is greater than $NS \times 100\%$ of the generation maximum number G_{max}, the mutation process uses three individuals ($\overrightarrow{x}_{r1}$, $\overrightarrow{x}_{r2}$, and $\overrightarrow{x}_{r3}$) from an External Archive instead of selecting them from the current population X (as in the traditional DE algorithm). Such selection is based on CD. Larger values of CD are preferred since they represent a measure to know uncovered regions of nondominated solutions. Therefore, more uniform Pareto front is obtained by using this diversity strategy.

Storing in the External Archive. This work uses an External Archive (ExA) to store the nondominated solutions along the search. The ExA allows finding better solutions when the diversity strategy based on CD is applied and thus accomplishes with design requirements appropriately [35]. The ExA allows the entrance of a solution if it is feasible and dominates any of the solutions inside the ExA. The dominated solutions from the ExA are removed. This process is expressed in the following definition.

Definition 6. Let $\overrightarrow{x_i} \in \mathbb{F}, \Longleftrightarrow f(\overrightarrow{x_i}) \prec f(\overrightarrow{z_j}) \mid \exists j = \{1, \ldots, S_F\}$, then x_i is accepted in the External Archive z and $z = z \setminus \{\overrightarrow{z_j}\}$, where S_F is the maximum solution numbers of External Archive.

This ExA is limited to a maximum number of nondominated solutions $n_{ExA_{MAX}}$. When the number of nondominated solutions n_{ExA} surpasses the maximum number of individuals in ExA $n_{ExA_{MAX}}$, the excesses of individuals $n_{ExA_{EXC}} = n_{ExA} - n_{ExA_{MAX}}$ are deleted. This removal of individuals is carried out equidistantly every $n_{ExA}/n_{ExA_{EXC}}$ of the nondominated solutions n_{ExA} in the ExA. Line 20 of the Algorithm 1 indicates the store and removal process of surplus solutions in ExA.

5. Results

The synergetic design problem of the bipedal lower-limb is solved by using the proposed multiobjective differential

evolution based on Multiselection Strategy explained in Section 4. Other four optimizers are implemented to compare the performance of the proposed optimizer. The first comparative DE-based multiobjective optimizer is denoted by "A1" which does not include either a strategy to promote diversity or a Multiselection Strategy [36]. The second DE-based multiobjective optimizer, denoted by "A2", uses the crowding distance to promote diversity and furthers elitism by the inclusion of the External Archive which stores nondominated solutions [31]. The third optimizer is termed as "A3" and is related to the proposed multiobjective differential evolution based on Multiselection Strategy. The fourth optimizer is the Nondominated Sorting Genetic Algorithm II (NSGA-II) [37] denoted by "A4". The last optimizer is the Multiobjective Particle Swarm Optimization (MOPSO) [38] termed as "A5". This includes boundary position update technique with absorb zero velocity update strategies [39] and also the best position of the swarm is taken from the knee solution of the Pareto front in the External Archive. The selection of the comparative optimizers is to provide enough information about the advantages of including the proposed Multiselection Strategy into the Multiobjective DE algorithm.

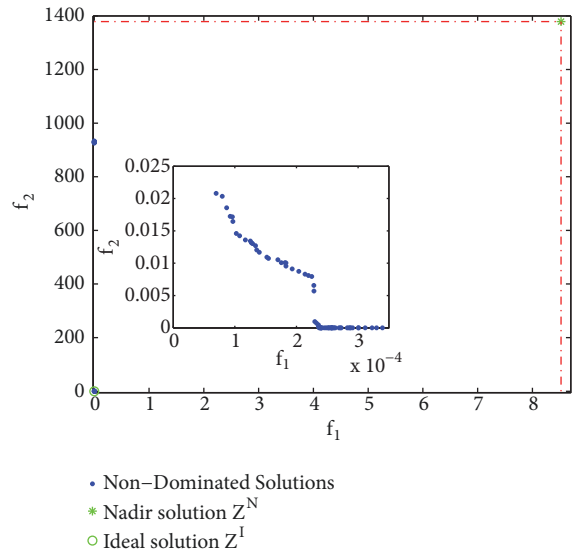

Figure 4: Global Pareto front with the Ideal Z^I and Nadir Z^N solution.

5.1. Comparative Analysis of Algorithms. An overall number of 25 independent runs of each algorithm are performed to obtain relevant information about their performance. In the case of DE-based optimizers, their parameters are set as follows: (i) the crossover probability is chosen as $CR = 0.65$. This was obtained through a trial and error procedure. (ii) The scale factor is randomly selected in the interval $F \in [0.3, 0.9]$ for each generation, as is described in [40]. (iii) The External Archive capacity is limited to $n_{ExA_{MAX}} = 200$ solutions with the Normal Selection of $NS = 0.3$ for algorithms "A2" and "A3". (iv) The population size and the maximum number of generations are set as NP = 20 and Gmax = 500000, respectively. In the case of "A4" and "A5", the optimizer parameters are chosen according to the recommended by the author cited. Only "A5" a population size of $NP = 200$ is selected. All algorithms are implemented in *MATLAB* over a PC with an i7-3.5 GHz CPU and 16 GB in RAM.

This work uses the normalized Hypervolume metric (HV) [33] to evaluate the performance in the diversity and convergence of the obtained Pareto front by using the five mentioned algorithms. This metric represents the normalized area covered by the Pareto front and a reference point. Whether the reference point is the Nadir vector, higher values of the HV metric indicate that the Pareto front has higher diversity and convergence to the True Pareto front. The Nadir vector is obtained by taking the worst independently objective function of the nondominated solutions for all algorithm runs. Since the True Pareto front is unknown in real-world engineering problems, in this work all resulting Pareto fronts from all algorithm runs are filtered to generate an approximation of the True Pareto front. The filtered process involves a dominance checking of all solutions given by runs and thus generates one single Pareto front. By using the approximation of the True Pareto front, the Ideal Z^I vector can be obtained with the best independently objective function of the nondominated solutions. Figure 4 shows the obtained approximation of the True Pareto front, where the Ideal $Z^I = [3.953e-5, 3.0873e-12]$ and Nadir $Z^N = [8.5219, 1379]$ vectors can be observed.

Table 3 shows the HV value of each algorithm execution, its mean value μ, and standard deviation σ. It is observed that the proposed algorithm "A3" presents more reliable results in the convergence and diversity of the obtained Pareto front because it presents larger mean value and standard deviation in HV metric.

In order to find significant differences among the performances of the five studied algorithms and to determine if those differences are not due to chance, the Wilcoxon signed-rank test is applied by pairs to the HV samples of each algorithm [41]. The "two-sided" alternative hypothesis is considered in this test, which establishes that the two samples have different distributions. The results of the Wilcoxon test are obtained with the statistical analysis software "R" and are shown in Table 4. In this table, R^+ indicates the positive rank sums, R^- shows the negative rank sums, and p denotes the rejection probability of the alternative hypothesis. The statistical significance of the test is set at 5%. Results in Table 4 confirm that the algorithm "A3" has the best performance compared with all other optimizers, followed by "A2" and "A4" which win two times, next "A1" wins one time, and the worst performance is given by "A5" due to the fact that this does not win in all comparison.

The above is due to the use of the Multiselection Strategy in "A3" enhancing the convergence towards desired regions of the objective function space. Additionally, the diversity is improved by including elite nondominated solutions from the External Archive (regarding the crowding distance) in the evolutionary operators. On the other hand, "A1" achieves the second worst Pareto fronts due to the fact that this algorithm only promotes the search space exploration by using random individuals from the population in the mutation process. The worst performance is "A5" algorithm and this is attributed

Table 3: Descriptive statistics of the Hypervolume by each algorithm.

Run	HV-A1	HV-A2	HV-A3	HV-A4	HV-A5
1	0.99880	0.99993	0.99987	0.99966	0.99668
2	0.99885	0.99952	1	0.99982	0.99753
3	0.99882	0.99981	0.99994	0.99940	0.99498
4	0.99884	0.99998	0.99997	0.99977	0.99366
5	0.99903	0.99975	0.99997	0.99955	0.99743
6	0.99893	0.99996	0.99989	0.99946	0.99220
7	0.99893	0.99975	0.99995	0.99935	0.99616
8	0.99907	0.99993	0.99998	0.99994	0.99794
9	0.99884	0.97618	0.99989	0.99994	0.99526
10	0.99890	0.99985	0.99985	0.99995	0.99732
11	0.97378	0.99979	0.99997	0.99980	0.99742
12	0.99880	0.99985	0.99996	0.99987	0.99784
13	0.99894	0.99986	0.99993	0.99982	0.99611
14	0.99895	0.99994	0.99996	0.99985	0.99730
15	0.99888	0.99978	0.99980	0.99996	0.99716
16	0.99916	0.99994	0.99984	0.99985	0.99650
17	0.99894	0.99976	0.99993	0.99986	0.99790
18	0.99889	0.99979	0.99985	0.99994	0.99772
19	0.99892	0.99975	0.99983	0.99988	0.99743
20	0.99890	0.99983	0.99994	0.99995	0.99060
21	0.99884	0.99975	0.99999	0.99919	0.99778
22	0.99887	0.99978	0.99997	0.99977	0.99820
23	0.99898	0.99976	0.99978	0.99976	0.99738
24	0.99900	0.99981	0.99994	0.99977	0.99772
25	0.99889	0.99977	0.99993	0.99986	0.99567
μ	0.998895	0.999789	0.999939	0.999820	0.997317
σ	0.004925	0.004633	0.000061	0.000204	0.001852

Table 4: Wilcoxon signed-rank test. Boldface words indicate the winners. "A3" wins four times. "A2" wins two times. "A4" wins two times. "A1" wins one time. "A5" does not win.

Wilcoxon test	R^+	R^-	$p-value$
A1 vs *A2*	24	301	0.00020
A1 vs *A3*	0	325	0.00001
A1 vs *A4*	0	325	0.00001
A1 vs A5	300	25	0.00022
A2 vs *A3*	26.5	273.5	0.00044
A2 vs A4	166	134	0.65780
A2 vs A5	300	25	0.00022
A3 vs A4	276.5	48.5	0.00023
A3 vs A5	325	0	0.00001
A4 vs A5	325	0	0.00001

to the lack of elitism because this algorithm does not include a selection process. Based on the above results, the algorithm "A3" is suitable to find Pareto fronts that allow the reconfigurability of the bipedal lower-limb with different synergistic levels in the design criteria.

Another performance metric evaluated in this paper is the Capacity Metric CM. This is related to the number of nondominated solutions (NDS) of the filtered Pareto front and in Table 5 this metric is shown as well as the Mean Convergence Time (MCT) of the 25 algorithm executions. The larger NDS (the best) is given by "A4". The second best is provided by the proposal "A3". The number of NDS obtained by "A3" is around 200%, 20%, and 900% greater than the number of NDS of "A1", "A2", and "A5", respectively. This indicates that "A3" presents a suitable NDS number. The MCT in algorithms that use larger NDS require more computational time to converge. Hence, the increment of MCT is related to the raise of NDS number.

Table 5: Number of nondominated solutions (NDS) and the Mean Convergence Time (MCT) of each algorithm.

Algorithm	NDS	MTC [h]
"A1"	26	2.45
"A2"	66	3.7
"A3"	81	4
"A4"	135	10.24
"A5"	8	1.5

Figure 5 shows the filtered Pareto front from all 25 runs per each algorithm. It visually confirms that the proposed

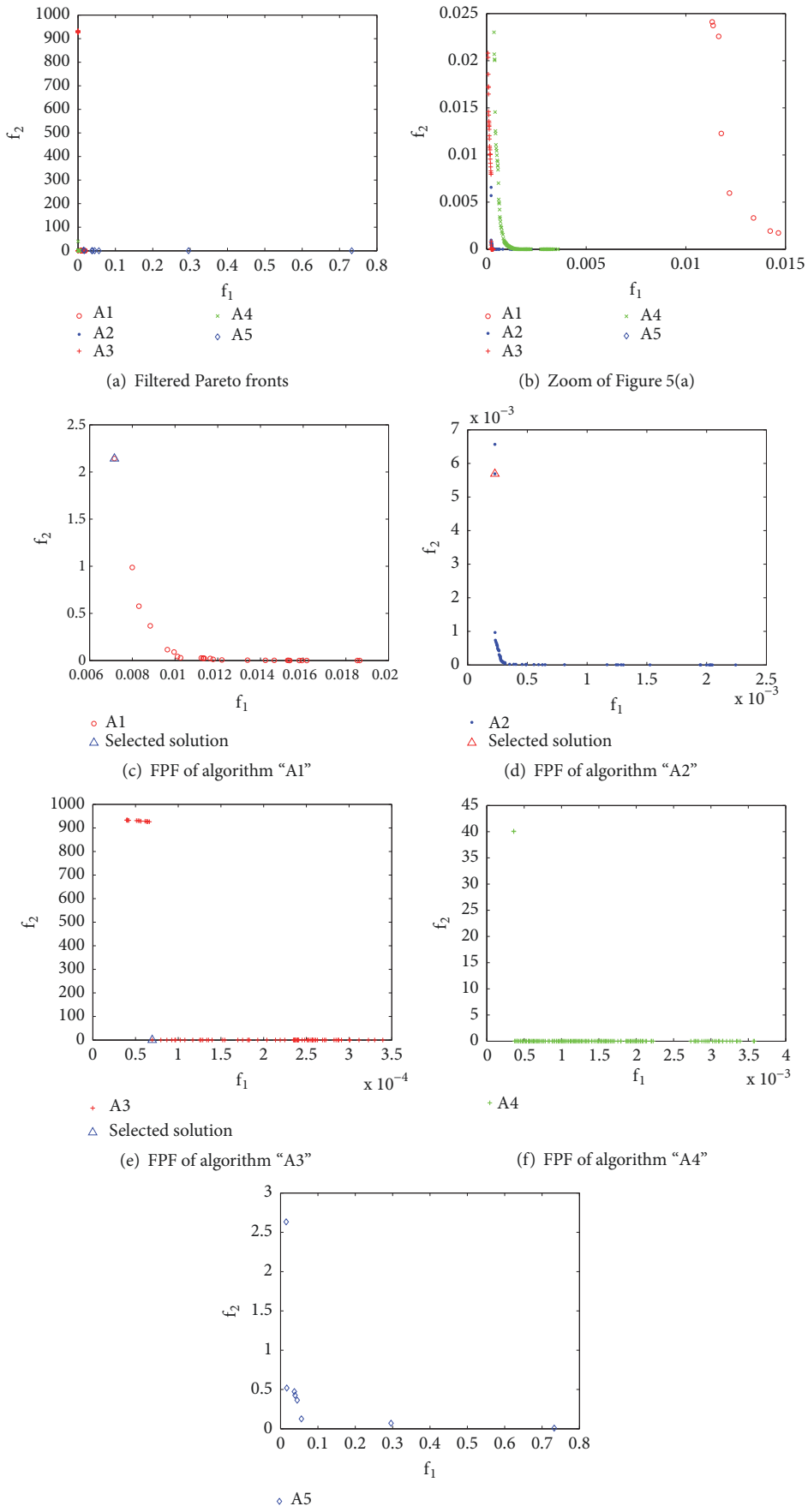

(a) Filtered Pareto fronts

(b) Zoom of Figure 5(a)

(c) FPF of algorithm "A1"

(d) FPF of algorithm "A2"

(e) FPF of algorithm "A3"

(f) FPF of algorithm "A4"

(g) FPF of algorithm "A5"

Figure 5: Filtered Pareto Front (FPF) set.

multiobjective differential evolution based on Multiselection Strategy "A3" has a better convergence level when is compared with the other algorithms; i.e., the Pareto solutions are closer to the objective function axes.

5.2. Optimal Design Solutions of the Bipedal Lower-Limb. In order to validate the bipedal lower-limb designs, a single alternative for the most representative algorithms is selected from the solutions observed in Figure 5. This selection is based on the two most reliable algorithms ("A2" and "A3") and the last one is chosen by considering the second worst algorithm ("A1"). This selection is performed by considering a desired trade-off between the objective functions f_1 and f_2. The selected designs prioritize low values of the performance function f_1; i.e., designs with higher accuracy in the bipedal gait path tracking are preferred since a highly desirable feature for the bipedal locomotion problem. With respect to the transmission angle deviation, the selected solutions must provide a low value of the performance function f_2 without abruptly increasing the value of the other performance function f_1. The selected alternatives for each algorithm are marked with a triangle in Figure 5. Table 6 shows the values of the design variables for the three selected designs and the corresponding objective function values. The obtained mechanisms from the above designs and their trajectories are depicted in Figure 6. Based on this figure, the expected behavior of the bipedal lower-limb designs (regarding the design criteria f_1 and f_2 shown in Table 6) is visually validated. With the above results, it is observed that the performance of the selected "A3" design in the bipedal gait path tracking overcomes the "A1" and "A2" selected designs although those solutions are obtained in the extreme of J_1 of the Pareto front. On the other hand, the force transmission related to the transmission angle deviation in the design "A3" is better than the design "A1" but worse than the design "A2". This indicates that the design solutions "A2" and "A3" are nondominated; nevertheless the best solution for the specific application, as is observed in Figure 6, is given by the design "A3".

Figure 7 shows the computer-aided design and the manufactured prototype of the bipedal lower-limb of the selected solution obtained by using the proposed multiobjective differential evolution based on Multiselection Strategy "A3". Furthermore, Figure 9 displays image sequences of the path tracking for that design. It is verified that the bipedal lower-limb suitably generates the desired gate cycle with a mean error of $1.7405E-3m$ from the desired points and with the mean transmission angle deviation error of $93.4215E-3rad$ from the $\pi/2$ value.

Finally, in Figure 8 depicts the conceptual design of a plow machine with the previous selected design. It is important to note that depending on the application, the designer can take the most suitable solution to satisfy the best trade-off for the specific task.

Table 6: Elite solutions by each algorithm.

$\mathbf{x}/f_1, f_2$	A1	A2	A3
l_1 (m)	0.143750	0.159943	0.168804
l_2 (m)	0.029883	0.026493	0.021943
l_3 (m)	0.152364	0.081143	0.132876
l_4 (m)	0.040659	0.106479	0.061185
l_5 (m)	0.181489	0.151873	0.195763
l_6 (m)	0.005493	0.018316	0.018670
l_7 (m)	0.139341	0.131240	0.179423
l_8 (m)	0.172391	0.108539	0.114913
l_9 (m)	0.048887	0.155669	0.104432
l_{11} (m)	0.164733	0.073504	0.136750
l_{12} (m)	0.175375	0.175156	0.107287
l_{14} (m)	0.166554	0.161790	0.168489
θ_1 (rad)	6.049799	5.231055	5.868656
θ_5 (rad)	3.437652	4.269796	3.508869
$\widehat{\theta_1}$ (rad)	1.984928	2.613263	0.181815
$\widehat{\theta_2}$ (rad)	1.501872	1.058254	1.635668
$\widehat{\theta_7}$ (rad)	5.469450	1.535836	4.230632
$\overline{x}_{ini}$ (m)	−0.132045	0.003473	−0.226627
m_{4b_1}	1	−1	−1
m_{4b_2}	1	1	1
m_{5b}	1	1	1
θ_2^1 (rad)	1.669011	2.879284	0.930970
θ_2^2 (rad)	3.279888	2.941268	1.107346
θ_2^3 (rad)	1.434247	3.061450	1.247409
θ_2^4 (rad)	5.026888	3.156033	1.360758
θ_2^5 (rad)	3.651130	3.291098	1.578239
θ_2^6 (rad)	3.305576	3.426843	1.688105
θ_2^7 (rad)	2.744528	3.585513	1.905511
θ_2^8 (rad)	3.724827	3.762008	2.193723
θ_2^9 (rad)	3.796385	3.916067	2.340580
θ_2^{10} (rad)	3.005416	4.295885	2.669695
θ_2^{11} (rad)	3.865946	4.670940	2.906157
θ_2^{12} (rad)	4.034493	5.270252	3.255427
θ_2^{13} (rad)	2.895384	5.835251	3.672310
θ_2^{14} (rad)	0.717203	0.102346	4.116944
θ_2^{15} (rad)	0.527806	0.403902	4.764391
θ_2^{16} (rad)	5.393533	2.331120	5.514985
θ_2^{17} (rad)	5.573647	2.518675	0.140237
θ_2^{18} (rad)	5.773207	2.614748	0.420469
θ_2^{19} (rad)	1.211520	2.711574	0.525204
θ_2^{20} (rad)	5.533811	2.768429	0.724136
f_1	0.007158	0.000228	0.000069
f_2	2.141981	0.005691	0.020800

6. Conclusions

In this paper, the synergistic design of continuous path generation and the force transmission of a bipedal lower-limb mechanism that fulfills twenty precision points of the gait cycle is stated as a Pareto-based Nonlinear Mixed Discrete-Continuous Constrained Multiobjective Optimization Problem to perform synergy between both design conflictive criteria. The task of selecting the a priori specific trade-off (as in the case of the weighed sum approach) is overcome due to the proposal, where a set of solutions capable of

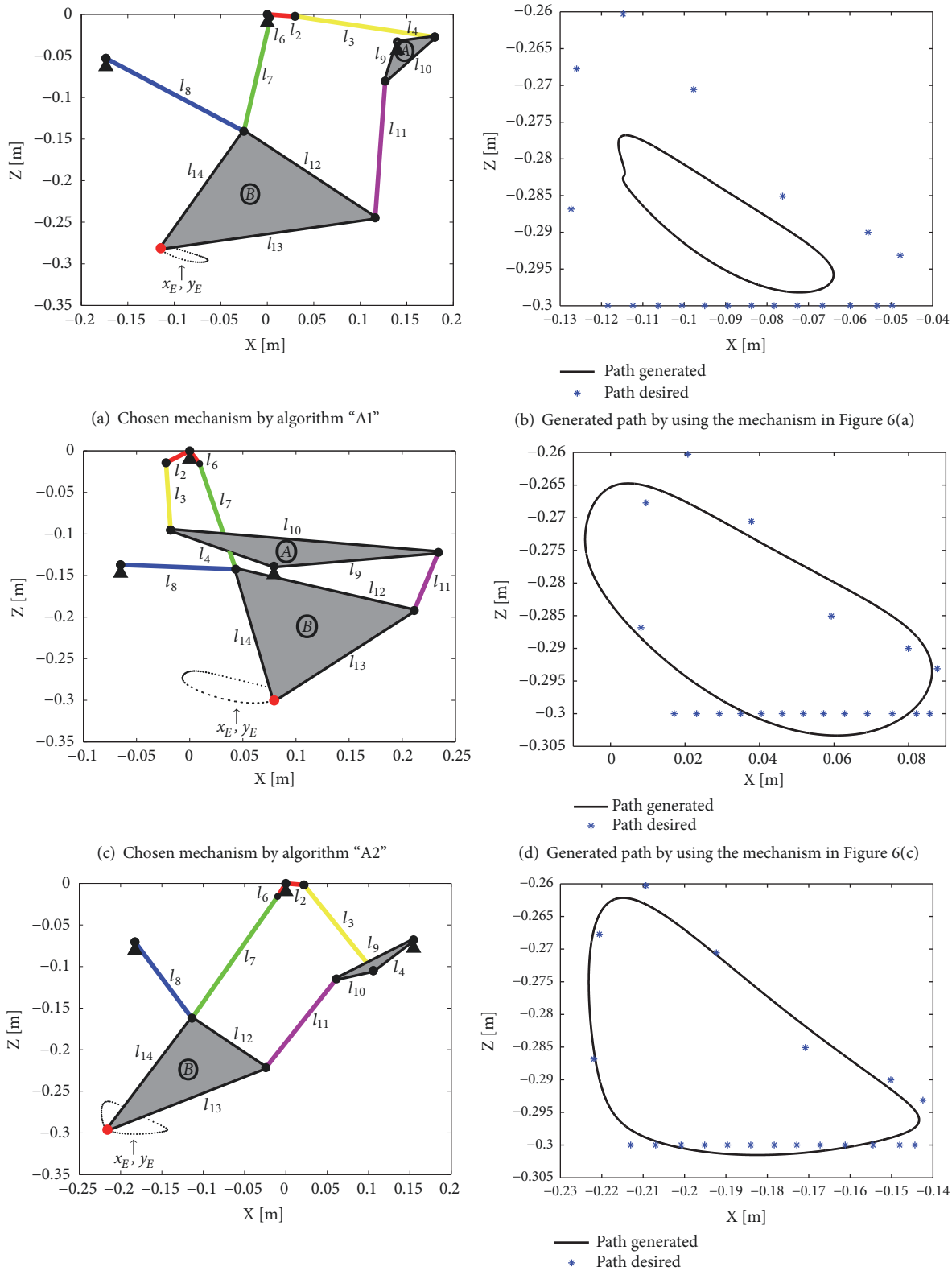

(a) Chosen mechanism by algorithm "A1"

(b) Generated path by using the mechanism in Figure 6(a)

(c) Chosen mechanism by algorithm "A2"

(d) Generated path by using the mechanism in Figure 6(c)

(e) Chosen mechanism by algorithm "A3"

(f) Generated path by using the mechanism in Figure 6(e)

Figure 6: Set of mechanisms and generated paths.

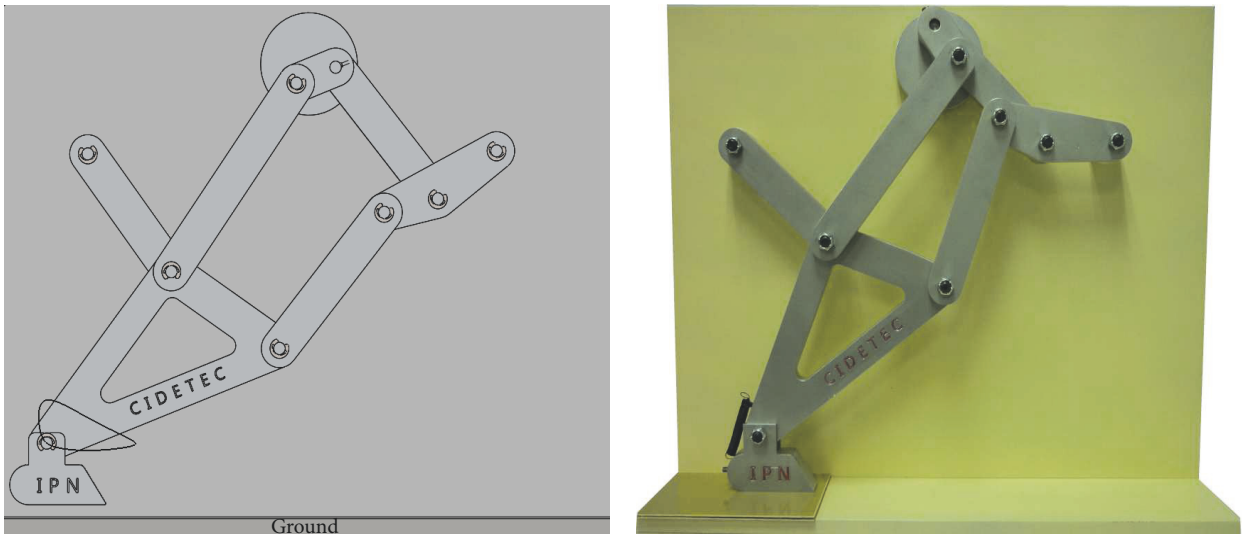

(a) CAD (b) Real mechanism

Figure 7: Bipedal lower-limb mechanism.

Figure 8: Virtual representation of a plow machine with the obtained design.

accomplishing the conflictive design criteria in the bipedal lower-limb design is obtained.

Moreover, the synergy is also considered in the optimizer by including a Multiselection Strategy into the selection process of the multiobjective differential evolution algorithm which promotes the discovery of better synergistic designs, with more quantity and diversity of solutions providing several design reconfigurability with different trade-offs to the designer decision making. This is because the proposed strategy enhances the search to a particular region (exploitation) of the Pareto front. The comparative statistical analysis based on the Hypervolume metric of the proposed Multiselection Strategy confirms that using the Multiselection Strategy, the External Archive and the diversity mechanism presented in this paper, improves the convergence, diversity, and widespread of the obtained Pareto solutions. Besides, the proposal provides a suitable set of nondominated solutions.

Data Availability

The data used to support the findings of this study are available from the corresponding author upon request.

Conflicts of Interest

The authors have declared that no conflicts of interest exist.

Acknowledgments

The first author acknowledges the support from the Consejo Nacional de Ciencia y Tecnología (CONACyT) through the scholarship to pursue his graduate studies at CIDETEC-IPN.

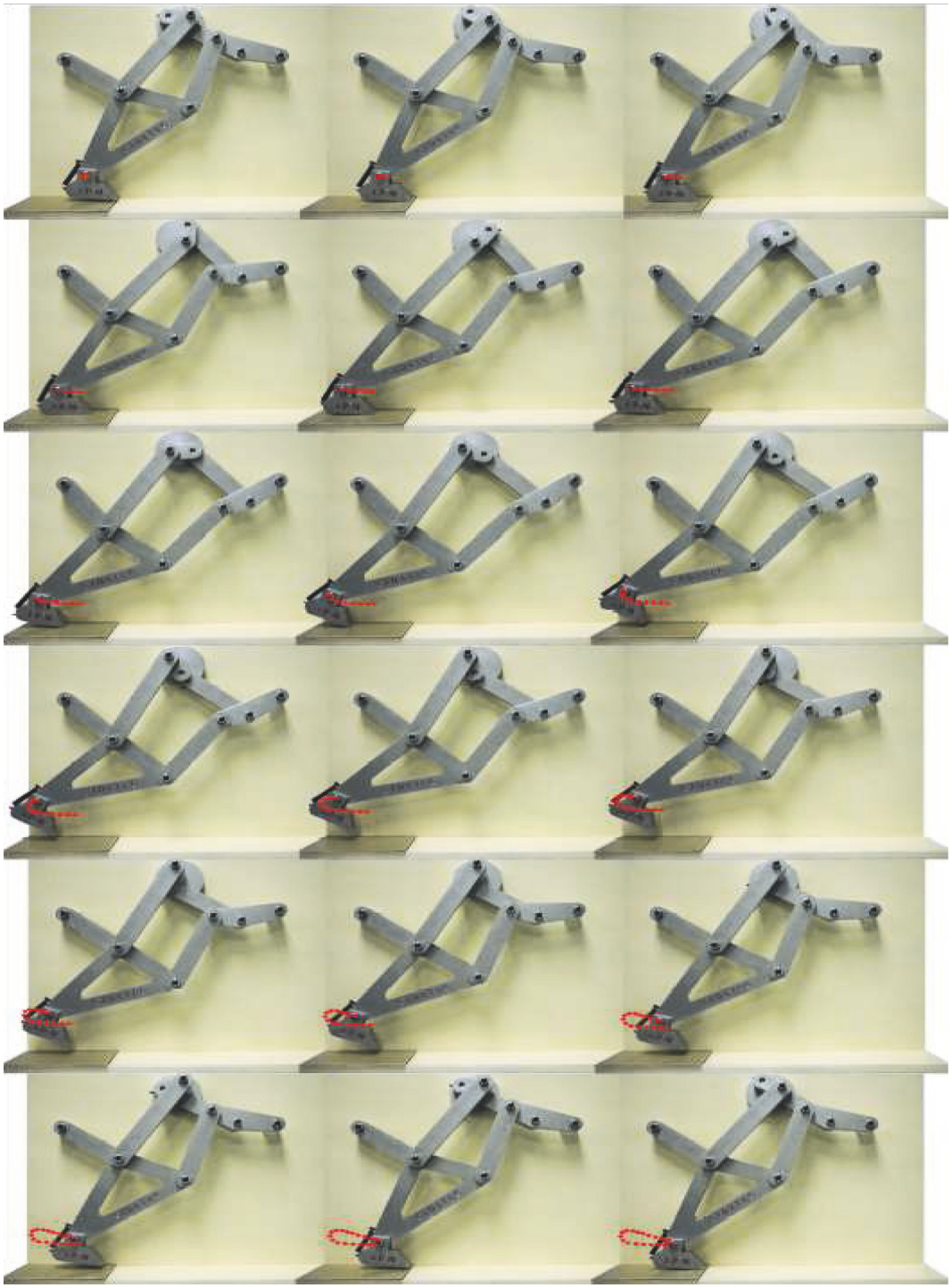

Figure 9: Frames of the bipedal lower-limb.

The authors acknowledge the support of the Secretaría de Investigación y Posgrado (SIP) through the Projects nos. SIP-20180196, SIP-20195279, and SIP-20195381.

References

[1] P. Mishra, A. Ahuja, and T. Shivpuri, "Mechatronics-concept of past core competence of future," *International Journal of Power Control Signal and Computation*, vol. 2, pp. 88–93, 2011.

[2] E. Gezgin, P.-H. Chang, and A. F. Akhan, "Synthesis of a Watt II six-bar linkage in the design of a hand rehabilitation robot," *Mechanism and Machine Theory*, vol. 104, pp. 177–189, 2016.

[3] G. Jang, C. Lee, H. Lee, and Y. Choi, "Robotic index finger prosthesis using stackable double 4-BAR mechanisms," *Mechatronics*, vol. 23, no. 3, pp. 318–325, 2013.

[4] P. Ávila-Hernández and F. Cuenca-Jiménez, "Design and synthesis of a 2 DOF 9-bar spatial mechanism for a prosthetic

thumb," *Mechanism and Machine Theory*, vol. 121, pp. 697–717, 2018.

[5] B. Y. Tsuge, M. M. Plecnik, and J. M. McCarthy, "Homotopy directed optimization to design a six-bar linkage for a lower limb with a natural ankle trajectory," *Journal of Mechanisms and Robotics*, vol. 8, no. 6, pp. 1–7, 2016.

[6] C. Copilusi, M. Ceccarelli, N. Dumitru, and G. Carbone, "Design and simulation of a leg exoskeleton linkage for a human rehabilitation system," in *Proceedings of the 11th IFToMM International Symposium on Science of Mechanisms and Machines*, I. Visa, Ed., vol. 18 of *Mechanisms and Machine Science*, pp. 117–125, Springer International Publishing, 2014.

[7] B. Y. Tsuge and J. M. McCarthy, "Synthesis of a 10-bar linkage to guide the gait cycle of the human leg," in *Proceedings of the ASME 2015 International Design Engineering Technical Conferences and Computers and Information in Engineering Conference, IDETC/CIE 2015*, USA, August 2015.

[8] M. B. Calva-Yanez, P. A. Nino-Suarez, E. A. Portilla-Flores, J. A. Aponte-Rodriguez, and E. Santiago-Valentn, "Reconfigurable mechanical system design for tracking an ankle trajectory using an evolutionary optimization algorithm," *IEEE Access*, vol. 5, pp. 5480–5493, 2017.

[9] O. Bozorg-Haddad, M. Solgi, and H. A. Loáiciga, *Meta-Heuristic and Evolutionary Algorithms for Engineering Optimization*, John Wiley & Sons, Inc., 2017.

[10] C. A. C. Coello, G. B. Lamont, and D. A. van Veldhuizen, "Evolutionary algorithms for solving multi-objective problems," in *Genetic and Evolutionary Computation*, Springer, New York, NY, USA, 2007.

[11] Y. Shao, Z. Xiang, H. Liu, and L. Li, "Conceptual design and dimensional synthesis of cam-linkage mechanisms for gait rehabilitation," *Mechanism and Machine Theory*, vol. 104, pp. 31–42, 2016.

[12] A. Bataller, J. A. Cabrera, M. Clavijo, and J. J. Castillo, "Evolutionary synthesis of mechanisms applied to the design of an exoskeleton for finger rehabilitation," *Mechanism and Machine Theory*, vol. 105, pp. 31–433, 2016.

[13] Z. Ji and Y. Manna, "Synthesis of a pattern generation mechanism for gait rehabilitation," *Journal of Medical Devices, Transactions of the ASME*, vol. 2, no. 3, 2008.

[14] A. J. McDaid, "Design, analysis, and multicriteria optimization of an overground pediatric robotic gait trainer," *IEEE/ASME Transactions on Mechatronics*, vol. 22, no. 4, pp. 1674–1684, 2017.

[15] R. Singh, H. Chaudhary, and A. K. Singh, "A novel gait-based synthesis procedure for the design of 4-bar exoskeleton with natural trajectories," *Journal of Orthopaedic Translation*, vol. 12, pp. 6–15, 2018.

[16] R. Singh, H. Chaudhary, and A. K. Singh, "Defect-free optimal synthesis of crank-rocker linkage using nature-inspired optimization algorithms," *Mechanism and Machine Theory*, vol. 116, pp. 105–122, 2017.

[17] Z. Shen, G. Allison, and L. Cui, "An integrated type and dimensional synthesis method to design one degree-of-freedom planar linkages with only revolute joints for exoskeletons," *Journal of Mechanical Design*, vol. 140, no. 9, 2018.

[18] J. S. Pantoja-García, M. G. Villarreal-Cervantes, J. C. González-Robles, and G. Sepúlveda-Cervantes, "Optimum synthesis of a biped gait mechanism using differential evolution," *Revista Internacional de Métodos Numéricos para Cálculo y Diseño en Ingeniera*, vol. 33, no. 1-2, pp. 138–153, 2017.

[19] Y. Collette and P. Siarry, *Multiobjective Optimization*, Decision Engineering, Springer-Verlag, Berlin, Germany, 2004.

[20] I. Das and J. E. Dennis, "A closer look at drawbacks of minimizing weighted sums of objectives for Pareto set generation in multicriteria optimization problems," *Journal of Structural Optimization*, vol. 14, no. 1, pp. 63–69, 1997.

[21] M. G. Villarreal-Cervantes, "Approximate and widespread Pareto solutions in the structure-control design of mechatronic systems," *Journal of Optimization Theory and Applications*, vol. 173, no. 2, pp. 628–657, 2017.

[22] D. W. Corne and J. D. Knowles, "No free lunch and free leftovers theorems for multiobjective optimisation problems," in *Proceedings of the 2nd International Conference on Evolutionary Multi-criterion Optimization, EMO'03*, vol. 2632 of *Lecture Notes in Computer Science*, pp. 327–341, Springer-Verlag, Berlin, Heidelberg, 2003.

[23] E. T. Wolbrecht, D. J. Reinkensmeyer, and A. Perez-Gracia, "Single degree-of-freedom exoskeleton mechanism design for finger rehabilitation," in *Proceedings of the Rehab Week Zurich 2011 - 2011 IEEE International Conference on Rehabilitation Robotics, ICORR 2011*, Switzerland, July 2011.

[24] G. Bovi, M. Rabuffetti, P. Mazzoleni, and M. Ferrarin, "A multiple-task gait analysis approach: Kinematic, kinetic and EMG reference data for healthy young and adult subjects," *Gait & Posture*, vol. 33, no. 1, pp. 6–13, 2011.

[25] S. S. Balli and S. Chand, "Transmission angle in mechanisms (Triangle in mech)," *Mechanism and Machine Theory*, vol. 37, no. 2, pp. 175–195, 2002.

[26] F. Grashof, "Theoretische maschinenlehre," *Leipzig: L. Voss*, vol. 2, 1875.

[27] R. M. Storn and K. V. Price, "Differential evolution - a simple and efficient adaptive shceme for global optimization over continuous spaces," Tech. Rep. TR-95-012, ICSI, 1995.

[28] T. Rogalsky, R. W. Derksen, and S. Kocabiyik, "Differential evolution in aerodynamic optimization," in *Proceedings of the 46th Annual Conference of the Canadian Aeronautics and Space Institute*, 1999.

[29] M. G. Villarreal-Cervantes, A. Rodriguez-Molina, C. Garcia-Mendoza, O. Penaloza-Mejia, and G. Sepulveda-Cervantes, "Multi-objective on-line optimization approach for the dc motor controller tuning using differential evolution," *IEEE Access*, vol. 5, pp. 20393–20407, 2017.

[30] S. Das and P. N. Suganthan, "Differential evolution: a survey of the state-of-the-art," *IEEE Transactions on Evolutionary Computation*, vol. 15, no. 1, pp. 4–31, 2011.

[31] E. A. Portilla-Flores, E. Mezura-Montes, J. Alvarez-Gallegos, C. A. Coello-Coello, C. A. Cruz-Villar, and M. G. Villarreal-Cervantes, "Parametric reconfiguration improvement in non-iterative concurrent mechatronic design using an evolutionary-based approach," *Engineering Applications of Artificial Intelligence*, vol. 24, no. 5, pp. 757–771, 2011.

[32] K. De Jong, *An Analysis of the Behavior of a Class of Genetic Adaptive Systems [Ph.D. thesis]*, University of Michigan, 1975.

[33] S. Jiang, Y.-S. Ong, J. Zhang, and L. Feng, "Consistencies and contradictions of performance metrics in multiobjective optimization," *IEEE Transactions on Cybernetics*, vol. 44, no. 12, pp. 2391–2404, 2014.

[34] K. Deb, "An efficient constraint handling method for genetic algorithms," *Computer Methods in Applied Mechanics and Engineering*, vol. 186, no. 2–4, pp. 311–338, 2000.

[35] E. Zitzler, K. Deb, and L. Thiele, "Comparison of multiobjective evolutionary algorithms: empirical results," *Evolutionary Computation*, vol. 8, no. 2, pp. 173–195, 2000.

[36] E. Mezura-Montes, M. Reyes-Sierra, and C. A. Coello-Coello, "Multi-objective optimization using differential evolution: a survey of the state-of-the-art," in *Advances in Differential Evolution*, pp. 173–196, Springer, 2008.

[37] K. Deb, A. Pratap, S. Agarwal, and T. Meyarivan, "A fast and elitist multiobjective genetic algorithm: NSGA-II," *IEEE Transactions on Evolutionary Computation*, vol. 6, no. 2, pp. 182–197, 2002.

[38] C. A. Coello Coello, G. T. Pulido, and M. S. Lechuga, "Handling multiple objectives with particle swarm optimization," *IEEE Transactions on Evolutionary Computation*, vol. 8, no. 3, pp. 256–279, 2004.

[39] E. Juárez-Castillo, N. Pérez-Castro, and E. Mezura-Montes, "Empirical study of bound constraint-handling methods in particle swarm optimization for constrained search spaces," in *Proceedings of the 2017 IEEE Congress on Evolutionary Computation (CEC)*, pp. 604–611, 2017.

[40] K. V. Price, R. M. Storn, and J. A. Lampinen, *Differential Evolution: A Practical Approach to Global Optimization*, Springer, Berlin, Germany, 2005.

[41] J. Derrac, S. García, D. Molina, and F. Herrera, "A practical tutorial on the use of nonparametric statistical tests as a methodology for comparing evolutionary and swarm intelligence algorithms," *Swarm and Evolutionary Computation*, vol. 1, no. 1, pp. 3–18, 2011.